

# Stability of Thin Liquid Sheet Flows

Marc W. McConley\*

*Massachusetts Institute of Technology, Cambridge, Massachusetts 02139*

Donald L. Chubb†

*NASA Lewis Research Center, Cleveland, Ohio 44135*

and

Matthew S. McMaster‡ and Abdollah A. Afjeh§

*University of Toledo, Toledo, Ohio 43606*

A two-dimensional, linear stability analysis of a thin nonplanar liquid sheet flow in vacuum is carried out. A sheet flow created by a narrow slit of  $W$  and  $\tau$  attains a nonplanar cross section as a consequence of cylinders forming on the sheet edge under the influence of surface tension forces. The region where these edge cylinders join the sheet is one of high curvature, and this is found to be the location where instability is most likely to occur. The sheet flow is found to be unstable, but with low growth rates for symmetric wave disturbances and high growth rates for antisymmetric disturbances. By combining the symmetric and antisymmetric disturbance modes, a wide range of stability characteristics is obtained. The product of unstable growth rate and flow time is proportional to the width-to-thickness ratio of the slit generating the sheet. Three-dimensional effects can alter these results, particularly when the sheet length-to-width ratio is not much greater than unity.

## Nomenclature

$A$	= area; disturbance amplitude
$c$	= wave propagation velocity
$k$	= wave number
$L$	= length of sheet
$M$	= dimensionless parameter related to stability parameter
$R$	= radius of curvature
$r$	= $x$ position at which end cylinder joins main sheet measured from the center of cylinder
$s$	= sheet-edge shape
$U$	= dimensionless $x$ velocity
$u, v, w$	= velocity components in Cartesian coordinate system
$W$	= slit width
$We$	= Weber number
$X, Y, Z$	= dimensionless parameters
$x, y, z$	= Cartesian coordinate system
$\beta$	= ratio of antisymmetric to symmetric disturbance amplitudes
$\gamma$	= dimensionless parameter
$\delta$	= stability parameter
$\zeta$	= dimensionless parameter related to stability parameter
$\lambda$	= wavelength
$\xi, \eta, \theta$	= dimensionless Cartesian coordinate system
$\rho$	= density
$\sigma$	= surface tension
$\tau$	= slit thickness
$\phi$	= velocity potential
$\psi$	= angle between antisymmetric waves and $z$ axis
$\omega$	= wave frequency

## Subscripts

asy	= antisymmetric
$c$	= end cylinder
$e$	= edge
max	= maximum value
$s$	= surface
sy	= symmetric
$x, y, z$	= partial derivatives with respect to, or components in, Cartesian coordinates
$\xi, \eta, \theta$	= partial derivatives with respect to, or components in, dimensionless Cartesian coordinates
0	= initial or steady-state value

## Introduction

STABILITY of incompressible, thin sheet flows has been of research interest for many years. Now there is renewed interest in sheet flows because of their possible application as low mass radiating surfaces.<sup>1–4</sup> Because of their low mass, near immunity to micrometeoroid damage, and simplicity, sheet flows are excellent candidates for a space radiator system. The objective of this study is to investigate the fluid dynamic stability of sheet flows that are of interest for a space radiator system. A stability parameter is derived to relate the product of the disturbance growth rate and the flow time of the system with other parameters of the flow.

Thin sheet flows are dominated by surface tension forces. As a result of surface tension at the edges of the sheet, a flow that begins with a dimension  $W$  perpendicular to the flow direction coalesces to a point at a distance  $L$  in the flow direction. The resulting triangular sheet is ideal for a space radiator. A sketch of the geometry of a thin liquid sheet flowing through a narrow slit at  $z = 0$  is shown in Fig. 1. Surface tension forces at the two edges of the sheet push the edges toward the  $z$  axis. As a result, as the flow moves in the  $z$  direction, the edge cross-sectional area  $A_e$  grows. To satisfy mass continuity, the edges approach each other and finally meet at the point  $z = L$ .

In the following two sections, the linear stability analysis will be developed. Following that, experimental results are compared to the theoretical results and an explanation for the discrepancy between the experimental and theoretical results is presented.

Received May 12, 1996; revision received June 5, 1996; accepted for publication June 12, 1996. Copyright © 1996 by the American Institute of Aeronautics and Astronautics, Inc. All rights reserved.

\*Graduate Student, Department of Aeronautical Engineering.

†Research Engineer, Photovoltaic Branch. Member AIAA.

‡Graduate Student, Department of Mechanical Engineering; currently at Virtual Engineering, St. Clair Shores, MI 48202.

§Professor, Mechanical Engineering Department. Member AIAA.

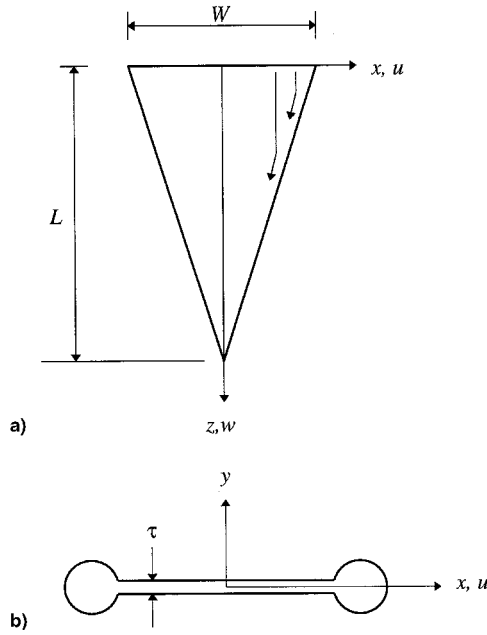


Fig. 1 Thin sheet flow: a) front and b) cross-sectional views.

### Linear Stability Analysis

It is well known<sup>5</sup> that a small-diameter cylindrical liquid jet becomes unstable and breaks up into drops as a result of surface tension. This surface-tension-driven instability was first described by Rayleigh.<sup>6</sup> For the case of thin, planar liquid sheets, however, the linearized theory, which applies to small disturbances of the sheet boundaries, does not yield any unstable solutions. Taylor<sup>7</sup> gives the solutions for two possible wave modes that may exist when a small disturbance is introduced into the flow. In the symmetric mode, displacements on opposite sides of the sheet are in opposite directions; in the antisymmetric mode, displacements on opposite sides of the sheet are in the same direction. Such waves are superimposed on the sheet cross section. Both wave modes are shown in Fig. 2.

If the liquid sheet is flowing into a gas rather than a vacuum, then the interaction of the gas and liquid will cause the sheet to break up. Squire<sup>8</sup> used a linear stability analysis to calculate the growth rate for thin sheets. Hagerty and Shea<sup>9</sup> considered finite thickness sheets. Later, Clark and Dombrowski,<sup>10</sup> using a second-order analysis, were able to calculate the breakup lengths of liquid sheets flowing into a gas. Recently, Rangel and Sirignano<sup>11</sup> completed a nonlinear stability analysis of this case. Crapper<sup>12</sup> obtained an exact solution for waves of arbitrary amplitude on a fluid of unlimited depth when surface tension is the only driving force. He obtains a result for the maximum wave amplitude (amplitude/wavelength = 0.73).

### Stability of a Nonplanar Liquid Sheet

Because of the sheet-edge shape, the sheet flows in this study are not planar. From Fig. 3 we can see that in the region where the constant thickness sheet joins the edge there is large curvature and, thus, large surface tension. Also, imperfections in the slits that are used to form the sheet flows produce nonplanar flow regions. It was expected that in these nonplanar regions unstable flow may occur. As a result, a linear stability analysis of a nonplanar sheet was carried out.

Dispersion relations for symmetric and antisymmetric waves are derived in Appendix A. This analysis uses equations for perturbation of the boundary  $\Delta s$  and velocity potential  $\Delta \phi$ , that are obtained from linearizing about the steady-state solutions  $s_0$  and  $\phi_0$ . Besides the usual neglecting of second-order terms in  $\Delta s$  and  $\Delta \phi$ , it was also assumed that the steady-state boundary velocities,  $u_{0,s}$  and  $v_{0,s}$ , are constant. This was done so that

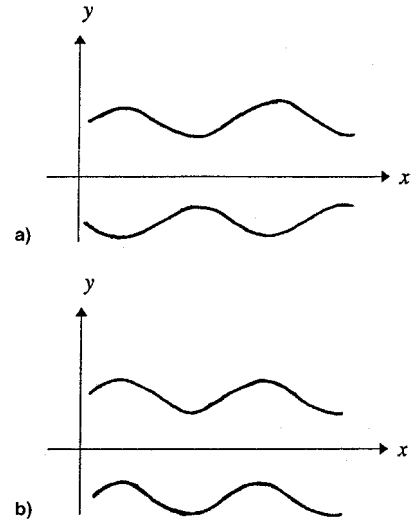


Fig. 2 Disturbance modes: a) symmetric and b) antisymmetric.

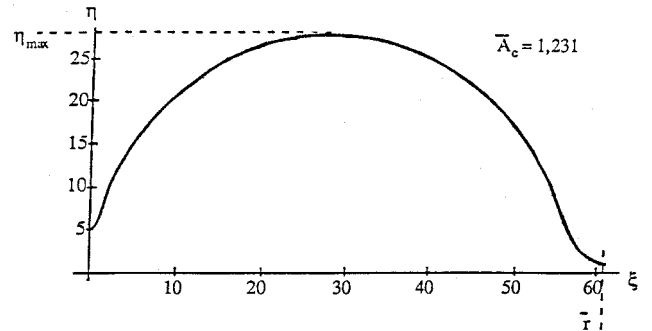


Fig. 3 Sample calculated cross section.

the usual traveling wave solution is applicable. In this analysis, the flow has been assumed to be two dimensional because the sheet length is typically much greater than the width of the slit, and we consequently expect gradients in the  $z$  direction to be small. Cases where this assumption does not hold will be discussed in the section on experimental results.

The dispersion relation for the symmetric wave is given by Eq. (A18), and for the antisymmetric wave by Eq. (A19). Here,  $\omega_{sy}$  is the complex frequency for symmetric waves,  $\omega_{asy}$  is the complex frequency for antisymmetric waves, and  $k$  is given by

$$k = 2\pi/\lambda \quad (1)$$

If either of the two roots for  $\omega_{sy}$  or  $\omega_{asy}$  have positive imaginary parts, then an unstable solution to Eq. (A11) for the boundary  $s$  exists. As Eqs. (A18) and (A19) indicate, if  $u_{0,s} = s_{0,x} = 0$ , then both  $\omega_{sy}$  and  $\omega_{asy}$  have only real roots, so that no unstable solutions exist. This is the result obtained by Taylor<sup>7</sup> for the planar sheet. In this case,  $s_0 = \tau_0/2$  and the phase velocities for the two waves are the following:

$$c_{sy} \equiv \frac{\omega_{sy}}{k} = \left[ \frac{2\pi\sigma}{\rho\lambda} \tanh\left(\frac{k\tau_0}{2}\right) \right]^{1/2} \quad (2a)$$

$$c_{asy} \equiv \frac{\omega_{asy}}{k} = \left[ \frac{2\pi\sigma}{\rho\lambda} \cosh\left(\frac{k\tau_0}{2}\right) \right]^{1/2} \quad (2b)$$

For thick sheets ( $k\tau_0/2 \rightarrow \infty$ ) the phase velocities are the same:

$$c_{sy} = c_{asy} = \sqrt{2\pi\sigma/\rho\lambda} \quad \left(\frac{1}{2}k\tau_0 \rightarrow \infty\right) \quad (3)$$

This agrees with the linear result given by Crapper<sup>12</sup> for  $\tau_0 \rightarrow \infty$ . Crapper's<sup>12</sup> exact result for waves of arbitrary amplitude  $A$  is

$$c_{sy} = c_{asy} = \sqrt{(2\pi\sigma/\rho\lambda)[1 + (\pi^2 A^2/4\lambda^2)]} \quad (\tau_0 \rightarrow \infty) \quad (4)$$

where  $A/\lambda \leq 0.73$ . Thus, for planar sheets, even for arbitrary amplitude, the phase velocity is closely approximated by the linear result.

For very thin planar sheets the phase velocities of the two waves differ significantly. For  $k\tau_0/2 \rightarrow 0$ , the antisymmetric wave phase velocity is the following:

$$c_{asy} = \sqrt{2\sigma/\rho\tau_0} = u_e \quad (\frac{1}{2}k\tau_0 \rightarrow 0) \quad (5a)$$

For the symmetric wave the phase velocity is the following:

$$c_{sy} = (2\pi/\lambda)\sqrt{\sigma\tau_0/2\rho} = (\pi\tau_0/\lambda)u_e \quad (\frac{1}{2}k\tau_0 \rightarrow 0) \quad (5b)$$

It has been found<sup>13</sup> that antisymmetric waves propagate at the rate at which the sheet edge moves toward the  $z$  axis. This rate is called the edge velocity  $u_e$ .

For the symmetric wave the phase velocity is small for thin sheets. However, for the antisymmetric wave the phase velocity is independent of the wavelength (no dispersion). This is similar to sound waves in a perfect gas or waves in an elastic string with tension  $2\sigma$  and mass per unit of length  $\rho\tau_0$ , as was pointed out by Taylor.<sup>7</sup> Lee and Wang<sup>14</sup> used the string analogy in analyzing a thin annular liquid jet.

Taylor<sup>7</sup> showed that the angle  $\psi$  that the lines of constant phase make with the vertical is given by

$$\psi = \sin^{-1}(c/w_0) \quad (6)$$

where  $w_0$  is the sheet velocity in the  $z$  direction and  $c$  is the wave phase velocity. Since  $c_{asy} = u_e$ , the lines of constant phase produced by antisymmetric waves must be parallel to the sheet edge, and this has been observed experimentally.<sup>13</sup> Since  $(\pi\tau/\lambda) \ll 1$ ,  $c_{sy} \gg c_{asy}$ , symmetric waves appear to be nearly vertical. Vertical waves, or striations, have been observed on the sheet as well. In general, the sheet is affected by both symmetric and antisymmetric disturbances.

Now consider the nonplanar sheet where the steady-state boundary velocities  $u_{0,x}$  and  $v_{0,x}$  are finite. For the steady-state solution the boundary condition given in Appendix B applies [Eq. (B4)].

If we define

$$X = ks_0, \quad Y = \omega' s_0/u_{0,x}, \quad \text{and} \quad \gamma = \sigma'/\rho u_{0,x}^2 s_0 \quad (7)$$

and neglect the slope in the  $y$ - $z$  plane so that

$$v_{0,x} = u_{0,x} s_{0,x} \quad (8)$$

then we may rewrite Eqs. (A18) and (A19) as follows:

$$Y_{sy}^2 + is_{0,x}(X \tanh X)Y_{sy} + \gamma X^3(is_{0,x} - \tanh X) = 0 \quad (9)$$

$$Y_{asy}^2 + is_{0,x}(X \coth X)Y_{asy} + \gamma X^3(is_{0,x} - \coth X) = 0 \quad (10)$$

Before presenting the general solutions for Eqs. (9) and (10), consider the solutions for the very thin sheet flows, i.e., the limiting condition  $X \rightarrow 0$ . From Eqs. (9) and (10)

$$\lim_{X \rightarrow 0} Y_{sy} = 0 \quad (11)$$

$$\lim_{X \rightarrow 0} Y_{asy} = -is_{0,x} \quad (12)$$

therefore

$$\lim_{X \rightarrow 0} \omega'_{asy} = -i(s_{0,x}u_{0,x}/s_0) - i(v_{0,x}/s_0) \quad (13)$$

which implies

$$\lim_{X \rightarrow 0} \omega_{i,asy} = \lim_{X \rightarrow 0} \text{Im}\{\omega'_{asy}\} \quad (14)$$

Thus, in the thin sheet limit there is no unstable symmetric solution. However, in the antisymmetric case the imaginary part of the frequency  $\omega_{asy}$  is nonzero, and either a decaying- or a growing-wave solution is possible. Since  $\Delta s \sim \exp[-i\omega t] \sim \exp[\omega_i t]$ , Eq. (14) indicates that an unstable solution will result, if and only if,  $v_{0,x} < 0$  in the upper half of the sheet for  $ks_0 \rightarrow 0$ . In the case of the sheet edge, this occurs in the region where the edge cylinder joins the sheet.<sup>13</sup> Experimentally, it has been found that holes develop in the sheet in this region.

In the purely symmetric case, the sheet flow is stable in the limit of infinite disturbance wavelength, but is slightly unstable for finite wavelengths. For wavelengths on the order of those exhibited by typical experimental flows, the unstable growth rate is usually too small to produce sufficient growth for hole formation before the fluid flows into the point of coalescence. In the purely antisymmetric mode, on the other hand, the sheet is predicted to be highly unstable in the region where the end cylinder joins the sheet. In the experimental flows studied, however, only occasional hole formation is usually observed, and sheets without holes can be formed. Hence, neither the antisymmetric nor the symmetric mode is sufficient alone to explain the observed sheet flow. Indeed, the nonlinear solutions of Clark and Dombrowski<sup>10</sup> for a liquid sheet in the atmosphere consist of both symmetric and antisymmetric modes. Mansour and Chigier<sup>15</sup> also observed both modes in their experiments.

#### Stability of Combined Symmetric and Antisymmetric Modes

If the sheet flow is affected by a disturbance consisting of both a symmetric and an antisymmetric mode, then the symmetric mode has a damping effect that tends to reduce the unstable growth rate below that of the purely antisymmetric mode. A stability parameter  $\delta$  is defined as

$$\delta \equiv t_f/t_i = (L/w_0)\omega_i = (W/2u_e)\omega_i \quad (15)$$

where  $t_f$  is the flow time (time for a fluid element to go from  $z = 0$  to  $z = L$ ) and  $t_i = 1/\omega_i = 1/\text{Im}\{\omega'\}$  is the growth rate of a disturbance. This parameter is used to measure the relative stability of the flow by indicating the amount of disturbance growth that can take place upstream of the point of coalescence: a disturbance amplitude will increase by a factor of  $e^\delta$  as the fluid travels from the slit to the point of coalescence. The stability parameter depends on three quantities: the sheet width-to-thickness ratio, the ratio of the sheet thickness to the disturbance wavelength, and the ratio of the antisymmetric amplitude to the symmetric amplitude.

To obtain  $\delta$ , we must derive the dispersion relation for combined symmetric and antisymmetric modes. From Appendix A, Eqs. (A16) and (A17) must be satisfied at the sheet-vacuum boundary. Solving Eqs. (A16) and (A17) simultaneously at the boundary ( $y = s_0$ ) yields

$$Y^2 + is_{0,x}\beta XY + \gamma X^3(is_{0,x} - \beta) = 0 \quad (16)$$

where  $X$ ,  $Y$ , and  $\gamma$  are given by Eq. (7) and

$$\beta = \frac{A_{asy} + A_{sy} \tanh ks_0}{A_{asy} \tanh ks_0 + A_{sy}} \quad (17)$$

It is straightforward to check that Eq. (16) reduces to Eq. (A18) for the symmetric case when  $A_{\text{asy}} = 0$  and to Eq. (A19) for the antisymmetric case when  $A_{\text{sy}} = 0$ .

In a typical thin sheet flow, the wavelength is considered large compared to the thickness of the sheet. In the limit of long wavelength ( $ks_0 \ll 1$ ), the solution for  $\omega$  to first order is

$$\omega' = \frac{u_{0,s}}{s_0} Y \rightarrow -ikv_{0,s} \left( \frac{A_{\text{asy}} + A_{\text{sy}}ks_0}{A_{\text{asy}}ks_0 + A_{\text{sy}}} \right) \quad (18)$$

The growth rate of disturbance waves is the imaginary part of  $\omega$ :

$$\omega_i = \text{Im}\{\omega\} = \text{Im}\{\omega'\} \rightarrow -kv_{0,s} \left( \frac{A_{\text{asy}} + A_{\text{sy}}ks_0}{A_{\text{asy}}ks_0 + A_{\text{sy}}} \right) \quad (19)$$

The solution is unstable if  $v_{0,s} < 0$ , just as it is for the anti-symmetric mode alone, since here,  $\omega_i > 0$ . In the pure symmetric limit,  $A_{\text{asy}} \rightarrow 0$ , and so  $\omega_i \rightarrow -k^2s_0v_{0,s}$ . Since  $ks_0 \rightarrow 0$ ,  $\omega_i$  approaches zero and the stable symmetric solution (11) is recovered. Similarly, if  $A_{\text{sy}} = 0$ , the disturbance is purely antisymmetric and  $\omega_i \rightarrow -v_{0,s}/s_0$ , which agrees with Eq. (14), the growth rate of the antisymmetric mode alone.

The parameter  $Y$  represents the growth rate of temporally varying disturbances. If this is large, i.e., the time constant of such growth is small compared with the flow time ( $\delta > 1$ ), then the sheet is said to be unstable because holes develop upstream of the point of coalescence. If the time constant is greater than, or on the order of, the flow time ( $\delta < 1$ ), then the sheet is said to be stable because no holes form upstream of the point of coalescence. Whether disturbances become large enough to produce holes depends in part on upstream fluctuations as well, so that a sheet with  $\delta$  somewhat greater than unity, but with only relatively small upstream perturbations, might still be free of holes.

To compute the stability parameter of the sheet, it is necessary to solve for the shape and surface velocities of the sheet edge. This is done in detail in Chubb et al.<sup>13</sup>; a summary of the relevant results is given here. In the course of the derivations, the  $x$  component of velocity  $u$  is assumed not to depend on  $y$ . Furthermore, the edge-shape solution is based on a two-dimensional theory, but experiments have revealed that three-dimensional effects also influence the edge shape.

To simplify the derivation, we introduce a number of dimensionless parameters

$$\xi \equiv \frac{x}{\tau/2}, \quad \eta \equiv \frac{s}{\tau/2}, \quad \theta \equiv \frac{z}{\tau/2}, \quad U_s \equiv \frac{u_s}{u_e}, \quad \bar{A} \equiv \frac{2A}{\tau^2} \quad (20)$$

where the subscript  $s$  indicates conditions at the surface boundary. Chubb et al.<sup>13</sup> showed that

$$U_s(\xi, \theta) = (1/\eta)[\bar{A}(\xi, \theta)/\bar{A}_c(\theta)] \quad (21)$$

The function  $\eta(\xi)$  was found to satisfy the following differential equation:

$$\eta_{\xi\xi} = \frac{1}{2(1+\alpha)} \left[ \frac{1}{\eta^2} \left( \frac{\bar{A}}{\bar{A}_c} \right)^2 (1 + \eta_\xi^2) - \frac{\tau}{R_e} \right] (1 + \eta_\xi^2)^{3/2} \quad (22)$$

where  $\alpha$  and  $\tau/R_e$  are uniquely determined based upon  $\bar{A}_c$ .  $\bar{A}$  is the dimensionless edge cylinder area integrated along the  $\xi$  axis and is a function of  $\xi$ . It is shown in Appendix B that  $\bar{A}_c$  is a linear function of  $z$ , and so  $\bar{A}_c$  is a linear function of  $\theta$ . Equation (22) must be solved numerically; a representative edge-shape solution is shown in Fig. 3.

If  $\delta$  is written in terms of the nondimensional variables of Eq. (20), incorporating  $\omega_i = (u_{0,s}/s_0)Y_i$  and  $Y_i = \text{Im}\{Y\}$ , the following is obtained:

$$\delta = Z_i(W/\tau) \quad (23)$$

where  $Z_i = \text{Im}\{Z\}$  and

$$Z = (1/\eta^2)(\bar{A}/\bar{A}_c)Y \quad (24)$$

Using Eq. (24) in Eq. (16), and expressing  $X$  and  $\gamma$  in terms of dimensionless variables, yields

$$\begin{aligned} Z^2 + i\beta \frac{\pi\eta_\xi}{\eta} \left( \frac{\bar{A}}{\bar{A}_c} \right) \left( \frac{\tau}{\lambda} \right) Z \\ + \pi^3 \left( \frac{\tau}{\lambda} \right)^3 (1 + \eta_\xi^2)^{-3/2} (i\eta_\xi - \beta) = 0 \end{aligned} \quad (25)$$

Solving Eq. (25) for  $Z$ , and taking the imaginary part, results in the stability parameter:

$$\begin{aligned} \delta = \frac{\zeta\beta}{2} \left\{ 1 + \frac{1}{\sqrt{2}} \left[ 1 - M \left( \frac{\tau}{\lambda} \right) \right. \right. \\ \left. \left. + \sqrt{1 - 2M \left( \frac{\tau}{\lambda} \right) + M^2 \left( 1 + \frac{\eta_\xi^2}{\beta^2} \right) \left( \frac{\tau}{\lambda} \right)^2} \right]^{1/2} \right\} \\ \times \left( \frac{\tau}{\lambda} \right) \left( \frac{W}{\tau} \right) \end{aligned} \quad (26)$$

where  $\beta$  is given by Eq. (17) and

$$\zeta = -\pi(\eta_\xi/\eta)(\bar{A}/\bar{A}_c) \quad (27)$$

$$M = [4\pi^3/(1 + \eta_\xi^2)](1/\beta\zeta^2) \quad (28)$$

The stability parameter depends on  $\zeta$ , which is a function only of the dimensionless coordinate  $\xi$ . The largest value of  $\delta$  occurs where  $\zeta$  is a maximum. This maximum occurs very close to the point where the edge cylinder joins the plane sheet ( $\xi = \bar{r}$  in Fig. 3). The maximum value  $\zeta_{\text{max}}$  was calculated based on the computed edge-shape solutions and is shown in Fig. 4. Note that  $\zeta_{\text{max}}$  is a function only of the dimensionless edge cross-sectional area  $\bar{A}_c$  (independent of fluid properties), and that  $\zeta$  is not a strong function of  $\bar{A}_c$  (except in a very small range of  $\bar{A}_c$ ). More rigorously,  $\zeta\bar{A}_c$  is approximately a linear function of  $\bar{A}_c$ , as demonstrated in Fig. 5. The results of Fig. 6 indicate that  $\zeta_{\text{max}} = 1.4$  is a good approximation over the range of  $\bar{A}_c$  of interest.

Consider the solution to Eq. (26) for the sheet flows of experimental interest. 1)  $\tau/\lambda \ll 1$  and 2)  $\tau/\lambda \ll A_{\text{asy}}/A_{\text{sy}}$  and  $\tau/\lambda \ll A_{\text{sy}}/A_{\text{asy}}$ , so that  $\beta \approx A_{\text{asy}}/A_{\text{sy}}$ . (If  $A_{\text{asy}}/A_{\text{sy}} \approx 1$ , and condition 1 is satisfied, condition 2 occurs automatically.)

Under these conditions, Eq. (26) can be expanded in a Taylor series. Retaining terms up to order  $(\tau/\lambda)^2$  produces the following result:

$$\delta = \zeta \left[ 1 - \frac{1}{4\pi} M \left( \frac{\tau}{\lambda} \right) \right] \left( \frac{\tau}{\lambda} \right) \left( \frac{W}{\tau} \right) \left( \frac{A_{\text{asy}}}{A_{\text{sy}}} \right) \quad (29)$$

Neglecting second-order terms in  $\tau/\lambda$  yields the following for  $\delta$ :

$$\delta = \zeta \left( \frac{\tau}{\lambda} \right) \left( \frac{W}{\tau} \right) \left( \frac{A_{\text{asy}}}{A_{\text{sy}}} \right) \quad \frac{\tau}{\lambda} \ll 1, \quad \beta \approx \frac{A_{\text{asy}}}{A_{\text{sy}}} \quad (30)$$

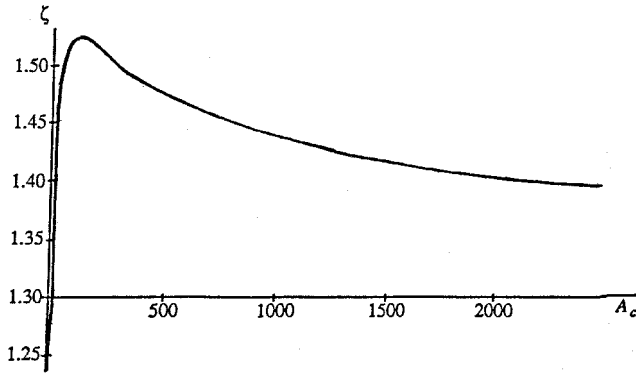


Fig. 4 Dependence of  $\zeta$  on end cylinder area.

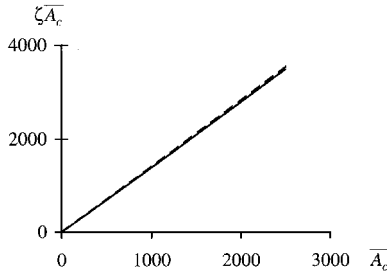


Fig. 5 Dependence of stability parameter on end cylinder. —, true  $\zeta A_c$  and ---, linear fit.

Using  $\zeta_{\max} = 1.4$ , the maximum stability parameter is the following:

$$\delta = 1.4 \left( \frac{\tau}{\lambda} \right) \left( \frac{W}{\tau} \right) \left( \frac{A_{\text{asy}}}{A_{\text{sy}}} \right) \quad \frac{\tau}{\lambda} \ll 1, \quad \beta \approx \frac{A_{\text{asy}}}{A_{\text{sy}}} \quad (31)$$

Recall that Eq. (30) and therefore, Eq. (31) are derived based on the assumption that  $\tau/\lambda \ll$  both  $A_{\text{asy}}/A_{\text{sy}}$  and  $A_{\text{sy}}/A_{\text{asy}}$ . For the pure symmetric or antisymmetric case, it is necessary to go back to Eq. (26). Note that  $A_{\text{asy}} = 0$  for the purely symmetric case, so that in the long wavelength limit

$$\begin{aligned} \beta &\rightarrow \tanh \left( \frac{\pi \tau}{\lambda} \eta \right) \rightarrow \frac{\pi \tau}{\lambda} \eta \Rightarrow \delta_{\text{sy}} \\ &\rightarrow \sqrt{\frac{-\pi^3 \eta_{\xi}}{2(1 + \eta_{\xi}^2)^{3/2}}} \left( \frac{W}{\tau} \right) \left( \frac{\tau}{\lambda} \right)^{3/2} = \zeta_{\text{sy}} \left( \frac{W}{\tau} \right) \left( \frac{\tau}{\lambda} \right)^{3/2} \end{aligned} \quad (32)$$

This applies only for  $\eta_{\xi} < 0$ , since only in that case is there instability ( $\omega_i > 0$ ). For long wavelengths,  $\delta_{\text{sy}} \rightarrow 0$ , thereby confirming that the sheet is stable for long wavelengths. The value of  $\zeta_{\text{sy}}$ , defined in Eq. (32), has been found to be approximately a constant equal to 2.443. The result of Eq. (32) was compared with the results of the full equation (26) for various  $\tau/\lambda$ . As shown in Fig. 6, appreciable discrepancy emerges for  $\tau/\lambda = 2 \times 10^{-2}$ , which is also where  $\delta > 1$ .

To demonstrate the relative stability of sheet flow with respect to symmetric disturbances, consider as an example a sheet flow produced by a slit  $3.44 \text{ cm} \times 75 \text{ } \mu\text{m}$ . Assume a pure symmetric disturbance with  $\tau/\lambda \approx 4 \times 10^{-3}$ . Substituting into Eq. (32) gives  $\delta = 2.443(W/\tau)(\tau/\lambda)^{3/2} = 0.28$ : the flow time is well below the growth time constant and the sheet is expected to be stable.

In the antisymmetric limit,  $A_{\text{sy}} = 0$ , so

$$\beta \rightarrow \coth \left( \frac{\pi \tau}{\lambda} \eta \right) \rightarrow \frac{\lambda}{\pi \tau \eta} \Rightarrow \delta_{\text{asy}} \rightarrow \left( \frac{-\eta_{\xi} \bar{A}}{\eta^2 \bar{A}_c} \right) \frac{W}{\tau} \approx 0.29 \frac{W}{\tau} \quad (33)$$

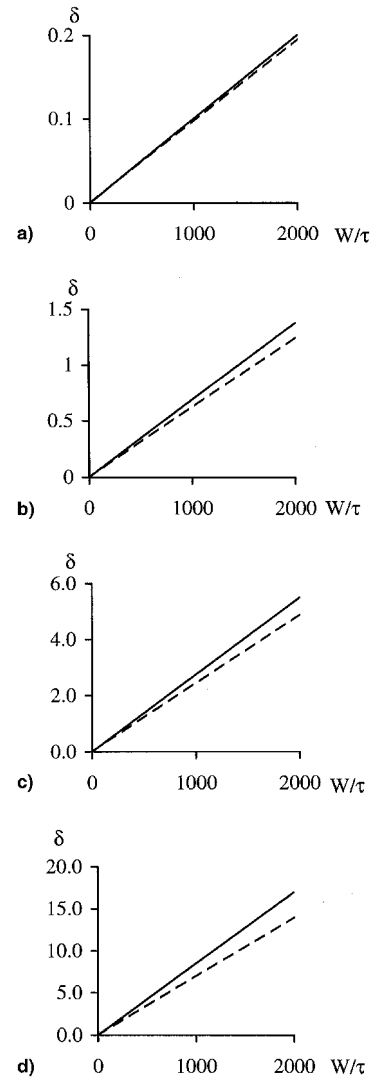


Fig. 6 Calculated stability parameter in pure symmetric mode.  $\tau/\lambda =$  a)  $1 \times 10^{-3}$ , b)  $4 \times 10^{-3}$ , c)  $1 \times 10^{-2}$ , and d)  $2 \times 10^{-2}$ . —, exact solution [Eq. (26)] and ---, approximate solution [Eq. (32)].

Since  $W/\tau \gg 1$  for a typical sheet, Eq. (33) confirms that a highly unstable sheet flow results if disturbances are purely antisymmetric. For example, in the case of the  $3.44 \text{ cm} \times 75 \text{ } \mu\text{m}$  slit,  $\delta = 130$ : the flow time is two orders of magnitude above the growth time constant. When Eq. (33) is compared with the result obtained by solving the full equation (26), very good agreement is found, and the error in the value of  $\delta$  is well below 1% for the range of wavelengths of interest.

A third special case exists if the symmetric and antisymmetric amplitudes are approximately the same. If  $A_{\text{asy}}/A_{\text{sy}} = 1$ , then  $\beta = 1$  for all values of  $\tau/\lambda$ , and Eq. (31) becomes

$$\delta_{\max} \approx 1.4 \frac{W}{\tau} \frac{\tau}{\lambda} \quad \frac{\tau}{\lambda} \ll 1, \quad \beta = 1 \quad (34)$$

For the previously considered slit example we obtain  $\delta = 2.6$ : the growth time is on the order of the flow time. From this we expect either stable sheet flow or only slightly unstable flow (occasional hole formation). Note that, if the vertical striations appearing on the sheet are the result of symmetric disturbance waves, then Eq. (34) is equivalent to  $\delta = 1.4n$ , where  $n$  is the number of striations on the sheet. Agreement of Eq. (34) with the result for  $\delta$  obtained by solving Eq. (26) is demonstrated in Fig. 7. Note that for the wavelengths of interest, agreement is quite good. The error in  $\delta$ , which arises as a result of the approximation Eq. (34), is about 10% when  $\tau/\lambda = 2 \times 10^{-2}$ .

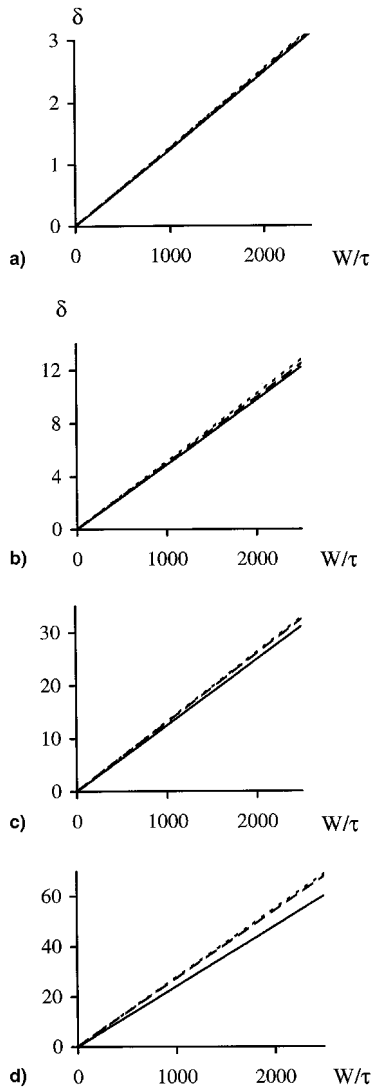


Fig. 7 Calculated stability parameter at  $\beta = 1$ .

### Comparison of Linear Stability Theory and Experimental Results

Recent experiments have produced sheets that seem to defy the analysis of the previous section. In researching the edge-shape geometry and the stability of these liquid sheet radiators, two different types of facilities have been used. The first is a large vacuum facility that uses diffusion pump oil (Dow-Corning 705 silicone oil) as the working fluid. This facility, which was used in previous studies,<sup>2,13</sup> does not have view ports that allow a view of the entire sheet. As a result, it is not suitable for studying hole formation. However, hole formation resulting from instability predicted by linear theory has been observed in these long sheet flows.

To view the entire sheet flow, a second smaller facility using water as the working fluid in air was constructed. This experiment used  $W = 20$  cm. The  $\tau$  could be varied continuously with a resolution of  $1 \mu\text{m}$ . The variable slit was attached to a large plenum that was connected to the city water supply through a control valve. A large plenum (plenum volume  $\gg$  sheet volume) is necessary to damp out pressure fluctuations produced by the water supply. If pressure fluctuations do occur upstream of the slit, holes will be produced in the sheet flow. Holes resulting from these fluctuations do not necessarily occur at the sheet edges. The results from this experiment defy the analysis of the previous section. For large  $W/\tau$ , that theory predicts instability, and sheets form that are free of holes.

Consider two sheets generated from the smaller experiment, with width-to-thickness ratios of 4000 and 4848 (length-to-width ratios of 1.6 and 1.2, respectively), both of which are completely devoid of holes. Theoretically, however, if we apply Eq. (35) for the stability parameter pertaining to the combined symmetric/antisymmetric disturbance, with an estimate for  $\tau/\lambda$  of  $4 \times 10^{-3}$ , we obtain  $\delta = 22.4$  when  $W/\tau = 4000$ . At this value of  $\delta$ , we expect the sheet to be highly unstable. In fact, even if we assume only symmetric disturbances and apply Eq. (32), we obtain  $\delta = 2.47$  for  $W/\tau = 4000$ , implying an order of magnitude increase ( $e^{2.47} = 12$ ) in the amplitude of small disturbances by the time the coalescence point is reached. It is not reasonable to assume that only symmetric disturbances are experienced, especially since antisymmetric disturbances have indeed been observed. Instead, we must conclude, at least in these cases, that our two-dimensional stability analysis is invalid.

One possible explanation of the discrepancy between the two experiments is that the second facility generally produces sheets of significantly lower length-to-width ratios. For small  $L/W$ , three-dimensional effects are more important since the edge cylinders are growing more rapidly than for  $L/W \gg 1$ . Therefore, the two-dimensional stability theory results are more likely to agree with the large  $L/W$  results than the small  $L/W$  results.

That three-dimensional effects become important for small  $L/W$  sheets is also suggested by measurements of the edge cylinder shapes for a sheet generated by the same facility. Figure 8, which is taken from Chubb et al.,<sup>13</sup> summarizes observations about the shapes of the edge cylinders made by photographing a sheet (length-to-width ratio of 2.62) from two different angles. Only the nearly circular shapes are predicted from a two-dimensional analysis (Fig. 3 and Chubb et al.<sup>13</sup>). Although the length-to-width ratio of 2.62 seems to be suffi-

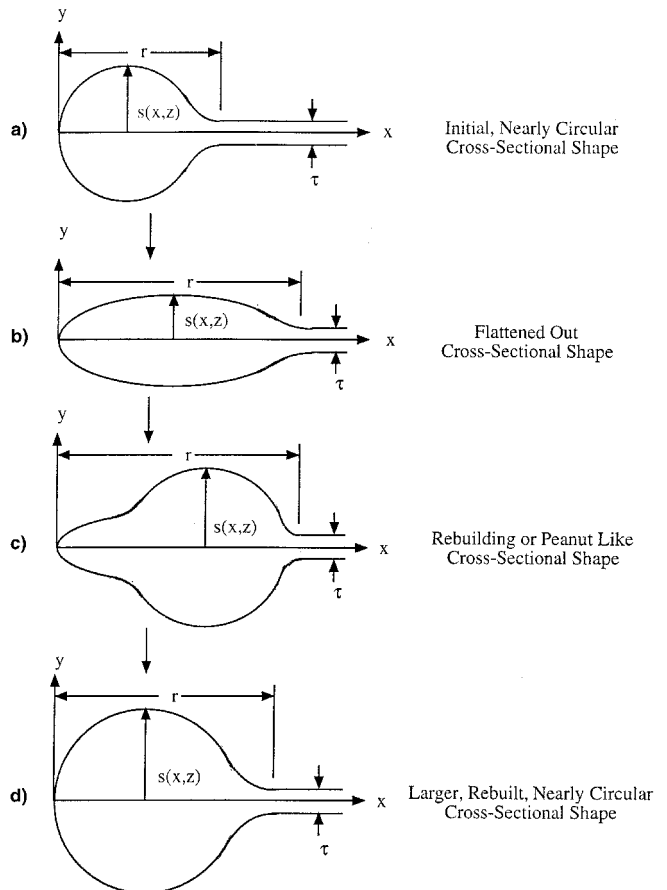


Fig. 8 Schematic diagram of edge cylinder variation in flow.  $\tau/\lambda =$  a)  $1 \times 10^{-3}$ , b)  $4 \times 10^{-3}$ , c)  $1 \times 10^{-2}$ , and d)  $2 \times 10^{-2}$ .

ciently larger than unity, it might be small enough that three-dimensional effects are important.

If the three dimensionality of the problem were taken into account, the disturbance growth rates could be fundamentally different from those derived in the two-dimensional analysis. If the sheet shapes of Fig. 8 are the result of three-dimensional effects, then it is reasonable to conclude that the sheets having length-to-width ratios of 1.6 and 1.2 are also significantly affected by three-dimensional effects. On the other hand, length-to-width ratios for sheets generated by the larger facility are on the order of 10 or 12, an order of magnitude higher than unity, and we expect the analysis to be closer to the experiment.

### Conclusions

In summary, the linear stability analysis for combined symmetric and antisymmetric modes yields a result for  $\delta$ . The value of this parameter compares well with experimental results using long ( $L/W \approx 10$ ) sheets in the larger facility. The symmetric mode alone predicts a  $\delta$  that is much too small, whereas the antisymmetric mode alone yields a  $\delta$  that is much too large. When both modes are combined in nearly equal amplitudes, the resulting value of  $\delta$  corresponds to a situation of occasional hole formation, as has been observed.

Three-dimensional effects might explain, at least in part, the stability of sheets formed from high  $W/\tau$  slits, but having low  $L/W$ . This is offered only as a suggestion; more experiments would be necessary to determine whether decreasing  $L/W$  indeed stabilizes the sheet, all else being held constant. A three-dimensional theoretical analysis of the edge cylinder shapes, a complex and tedious computational procedure to be sure, might provide additional insight.

The results of this study, both theoretical and experimental, are nonetheless encouraging. Where the theory and experiment are not in agreement, sheets are fortunately more stable than the theory predicts. Thus, the stability parameter might be treated as an upper bound on the growth rate of disturbances on liquid sheets. Most important, it has been determined that stable sheets, free of holes and suitable for use in a space radiator, can be generated.

### Appendix A: Dispersion Relations for Small Amplitude Waves on Nonplanar Sheet

We neglect the  $z$ -direction gravitational force and any curvature of the sheet in the  $y$ - $z$  plane. Therefore, assuming the liquid sheet is incompressible and irrotational the flow is governed by

$$\frac{\partial^2 \phi}{\partial x^2} + \frac{\partial^2 \phi}{\partial y^2} = 0 \quad (\text{A1})$$

subject to the following conditions at the vacuum-sheet boundary.

Bernoulli equation

$$\frac{d\phi}{dt} + \frac{1}{2} (u_s^2 + v_s^2) \pm \frac{\sigma}{\rho} \frac{s_{xx}}{(1 + s_{xx}^2)^{3/2}} = \text{const} \quad (\text{A2})$$

Boundary velocity = fluid velocity

$$\frac{ds}{dt} = v_s \Rightarrow \frac{\partial s}{\partial t} + u_s s_x = \frac{\partial \phi}{\partial y} \Big|_s \quad (\text{A3})$$

where

$$s_x = \frac{\partial s}{\partial x}, \quad \text{and} \quad s_{xx} = \frac{\partial^2 s}{\partial x^2} \quad (\text{A4})$$

The sign in front of the last term on the left-hand side of Eq. (A2) is negative for the upper half of the sheet ( $s > 0$ ), and positive for the lower half of the sheet ( $s < 0$ ).

Now linearize Eqs. (A1–A3) by substituting the following expressions for  $\phi(x, y, t)$  and  $s(x, t)$ :

$$\phi = \phi_0(x, y) + \Delta\phi(x, y, t) \quad (\text{A5})$$

$$s = s_0(x) + \Delta s(x, t) \quad (\text{A6})$$

where  $\phi_0$  and  $s_0$  are the steady-state solutions, and  $\Delta\phi$  and  $\Delta s$  are small perturbations from the steady-state solutions. Substituting Eqs. (A5) and (A6) in Eqs. (A1–A3) yields

$$\frac{\partial^2(\Delta\phi)}{\partial x^2} + \frac{\partial^2(\Delta\phi)}{\partial y^2} = -\frac{\partial^2\phi_0}{\partial x^2} - \frac{\partial^2\phi_0}{\partial y^2} = 0 \quad (\text{A7})$$

$$\frac{\partial(\Delta\phi_s)}{\partial t} + u_{0s} \frac{\partial(\Delta\phi_s)}{\partial x} + v_{0s} \frac{\partial(\Delta\phi_s)}{\partial y} - \frac{\sigma}{\rho} \frac{(\Delta s)_{xx}}{(1 + s_{0xx}^2)^{3/2}} = 0 \quad (\text{A8})$$

$$\frac{\partial(\Delta s)}{\partial t} + u_{0s} \frac{\partial(\Delta s)}{\partial x} + s_{0xx} \frac{\partial(\Delta\phi_s)}{\partial x} = \frac{\partial(\Delta\phi_s)}{\partial y} \quad (\text{A9})$$

Here,  $u_0$  and  $v_0$  are the steady-state velocity components,  $s_{0,x}$  is the steady-state slope of the boundary in the  $x$ - $y$  plane, and the subscript  $s$  denotes conditions at the boundary. In obtaining Eqs. (A8) and (A9), second-order terms in  $\Delta\phi$  and  $\Delta s$  have been neglected and the steady-state solutions have been eliminated.

Now assume wavelike solutions for  $\Delta\phi$  and  $\Delta s$ :

$$\Delta\phi = \hat{\phi}(y)e^{i(kx - \omega t)} \quad (\text{A10})$$

$$\Delta s = \hat{s}e^{i(kx - \omega t)} \quad (\text{A11})$$

Substituting Eq. (A10) in Eq. (A7) yields

$$\frac{\partial^2 \hat{\phi}}{\partial y^2} - k^2 \hat{\phi} = 0 \quad (\text{A12})$$

This has the following solution:

$$\hat{\phi} = A_{asy} \sinh ky + A_{sy} \cosh ky \quad (\text{A13})$$

where  $A_{asy}$  and  $A_{sy}$  are constants. There are two types of wave solutions to consider. In the symmetric wave solution (Fig. 3a),  $v = v_s$  on the upper boundary and  $v = -v_s$  on the lower boundary. For the antisymmetric case (Fig. 3b),  $v = v_s$  on both the upper and lower boundaries. Assuming  $\Delta s \ll s_0$ , the following results are obtained. For the symmetric case

$$\Delta\phi_{sy} = (A_{sy} \cosh ky)e^{i(kx - \omega t)} \quad (\text{A14})$$

and for the antisymmetric case

$$\Delta\phi_{asy} = (A_{asy} \sinh ky)e^{i(kx - \omega t)} \quad (\text{A15})$$

Using Eqs. (A10) and (A11) in Eqs. (A8) and (A9) gives

$$-i\omega' \hat{\phi} + v_{0s} \hat{\phi}_y + (\sigma'/\rho) k^2 \hat{s} = 0 \quad (\text{A16})$$

$$\omega' \hat{s} = k s_{0,x} \hat{\phi} + i \hat{\phi}_y \quad (\text{A17})$$

where  $\hat{\phi}_y = \partial \hat{\phi} / \partial y$ ,  $\omega' = \omega - k u_{0s}$ , and  $\sigma' = \sigma(1 + s_{0,x}^2)^{-3/2}$ . Substituting Eqs. (A14) and (A15) and solving Eqs. (A16) and (A17) simultaneously at the boundary ( $y = s_0$ ), yields the fol-

lowing dispersion relations for the symmetric and antisymmetric cases. For the symmetric case

$$(\omega'_{sy})^2 + ikv_{0,s}(\tanh ks_0)\omega'_{sy} + k^3(\sigma'/\rho)(is_{0,x} - \tanh ks_0) = 0 \quad (A18)$$

and for the antisymmetric case

$$(\omega'_{asy})^2 + ikv_{0,s}(\coth ks_0)\omega'_{asy} + k^3(\sigma'/\rho)(is_{0,x} - \coth ks_0) = 0 \quad (A19)$$

In applying Eqs. (A16) and (A17) at the boundary, it was assumed that  $s = s_0 + \Delta s \approx s_0$ . Also, the steady-state boundary velocities  $u_{0,s}$  and  $v_{0,s}$  have been assumed constant, so that the assumed wave solutions with constant  $k$  and  $\omega$  are applicable.

## Appendix B: Continuity Equation Solution

The continuity equation for steady-state incompressible flow is the following:

$$\frac{\partial u}{\partial x} + \frac{\partial v}{\partial y} + \frac{\partial w}{\partial z} = 0 \quad (B1)$$

where  $u$ ,  $v$ , and  $w$  are, respectively, the  $x$ -,  $y$ -, and  $z$ -direction velocities. Referring to Fig. 2, if Eq. (B1) is integrated from  $0 \leq y \leq s(x, z)$ , then Eq. (B1) becomes the following:

$$\frac{\partial s\bar{u}}{\partial x} + \frac{\partial s\bar{w}}{\partial z} + v_s - u_s \frac{\partial s}{\partial x} - w_s \frac{\partial s}{\partial z} = 0 \quad (B2)$$

where  $\bar{u}$  and  $\bar{w}$  are average velocities defined as follows:

$$\bar{u} = \frac{1}{s} \int_0^s u \, dy \quad \bar{w} = \frac{1}{s} \int_0^s w \, dy \quad (B3)$$

Since the flow is symmetric about the  $x$  axis,  $v(y=0) = 0$ .

At the sheet surface the fluid  $y$ -direction velocity  $v_s$  must equal the surface speed  $ds/dt$ . Therefore, for steady-state conditions

$$\frac{ds}{dt} = u_s \frac{\partial s}{\partial x} + w_s \frac{\partial s}{\partial z} = v_s \quad (B4)$$

Using Eq. (B4) in Eq. (B2) yields the following:

$$\frac{\partial(s\bar{u})}{\partial x} + \frac{\partial(s\bar{w})}{\partial z} = 0 \quad (B5)$$

If the gravity force and surface tension force (curvature in the  $y$ - $z$  plane) in the  $z$  direction are neglected, then  $\bar{w}_z \ll \bar{u}_x$ , where the subscripts denote partial differentiation. Therefore

$$\frac{\partial s\bar{u}}{\partial x} = -\bar{w} \frac{\partial s}{\partial z} \quad (B6)$$

Beginning at  $x = 0$ , where  $s = 0$  and  $\bar{u} = 0$ , integrate with respect to  $x$  to obtain

$$s\bar{u} = -\frac{1}{2} \bar{w} \frac{\partial A}{\partial z} \quad (B7)$$

where  $A$ , the sheet-edge cross-sectional area for  $0 \leq x' \leq x$  (see Fig. 2), is given by

$$A(x, z) = 2 \int_0^x s(x', z) \, dx' \quad (B8)$$

At the point  $x = r(z)$ , where the end cylinder joins the sheet, we have  $A = A_c$  and  $s\bar{u} = -(\tau/2)u_e$ , where  $A_c$  is the total sheet-edge cross-sectional area. Therefore, from Eq. (B7)

$$\tau u_e = \bar{w} \frac{dA_c}{dz} = \frac{dA_c}{dt} \quad (B9)$$

Since the gravity force and  $z$ -direction surface tension force are being neglected,  $u_e$ ,  $\bar{w} = w_0$ , and  $\tau = \tau_0$  are constants. Therefore, from Eq. (B9)

$$A_c(z) = 2 \int_0^{r(z)} s(x, z) \, dx = \frac{\tau_0 u_e}{w_0} z = \tau_0 z \sqrt{2We} \quad (B10)$$

where  $We$  is defined as  $\sigma/\rho w_0^2 \tau_0$ , and  $u_e$  is replaced by  $u_e = \sqrt{2\sigma/\rho\tau_0}$ .<sup>13</sup>

## Acknowledgment

The authors thank James Zakany for his assistance with the large facility experimental work for this project.

## References

- <sup>1</sup>Chubb, D. L., and White, K. A., "Liquid Sheet Radiator," AIAA Paper 87-1525, July 1987; also NASA TM-89841, July 1987.
- <sup>2</sup>Chubb, D. L., and Calfo, F. D., "Scaling Results for the Liquid Sheet Radiator," 24th Intersociety Energy Conversion Engineering Conf., Washington, DC, Aug. 1989; also NASA TM-10210, Aug. 1989.
- <sup>3</sup>Juhasz, A. J., and Chubb, D. L., "Design Considerations for Space Radiators Based on the Liquid Sheet (LSR) Concept," 26th Intersociety Energy Conversion Engineering Conf., Boston, MA, Aug. 1991; also NASA TM-10515, Aug. 1991.
- <sup>4</sup>Chubb, D. L., Calfo, F. D., and McMaster, M. S., "Current Status of Liquid Sheet Radiator Research," 1st International Conf. on Aerospace Heat Exchanger Technology, Palo Alto, CA; also NASA TM-105764, July 1993.
- <sup>5</sup>Drazin, P. G., and Reid, W. H., *Hydrodynamic Stability*, Cambridge Univ. Press, New York, 1981, pp. 22–27.
- <sup>6</sup>Rayleigh, Lord, *The Theory of Sound*, 2nd ed., Vol. 11, Dover, New York, 1945.
- <sup>7</sup>Taylor, Sir Geoffrey, "The Dynamics of Thin Sheets of Fluid II. Waves on Fluid Sheets," *Proceedings of the Royal Society of London, Series A: Mathematical and Physical Sciences*, Vol. 253, Dec. 1959, pp. 296–312.
- <sup>8</sup>Squire, H. B., "Investigation of the Instability of a Moving Liquid Film," *British Journal of Applied Physics*, Vol. 4, 1953, pp. 167–169.
- <sup>9</sup>Hagerty, W. W., and Shea, J. F., "A Study of the Stability of Plane Fluid Sheets," *Journal of Applied Mechanics*, Vol. 22, Dec. 1955, pp. 509–514.
- <sup>10</sup>Clark, C. J., and Dombrowski, N., "Aerodynamic Instability and Disintegration of Inviscid Liquid Sheets," *Proceedings of the Royal Society of London, Series A: Mathematical and Physical Sciences*, Vol. 329, May–Sept. 1972, pp. 467–478.
- <sup>11</sup>Rangel, R. H., and Sirignano, W. A., "The Linear and Nonlinear Shear Instability of a Fluid Sheet," *Physics of Fluids*, Vol. A3, No. 10, 1991, pp. 2392–2400.
- <sup>12</sup>Crapp, G. D., "An Exact Solution for Progressive Capillary Waves of Arbitrary Amplitude," *Journal of Fluid Mechanics*, Vol. 2, Pt. 3, 1957, pp. 532–540.
- <sup>13</sup>Chubb, D. L., Calfo, F. D., McConley, M. W., McMaster, M. S., and Afjeh, A. A., "The Geometry of Thin Liquid Sheet Flows," *AIAA Journal*, Vol. 3, No. 6, 1994, pp. 1325–1328.
- <sup>14</sup>Lee, C. P., and Wang, T. G., "A Theoretical Model for the Annular Jet Instability," *Physics of Fluids*, Vol. 29, No. 7, 1986, pp. 2076–2085.
- <sup>15</sup>Mansour, A., and Chigier, N., "Dynamic Behavior of Liquid Sheets," *Physics of Fluids*, Vol. A3, Nov. 1991, pp. 2971–2976.